6th IEEE RAS/EMBS International Conference on
Biomedical Robotics and Biomechatronics (BioRob)
June 26-29, 2016. UTown, Singapore

Evaluation of an Electromagnetic System with Haptic Feedback for Control of Untethered, Soft Grippers Affected by Disturbances

Federico Ongaro, Claudio Pacchierotti, ChangKyu Yoon,
Domenico Prattichizzo, David H. Gracias, and Sarthak Misra

Abstract— **Current wireless, small-scale robots have restricted manipulation capabilities, and limited intuitive tools to control their motion. This paper presents a novel teleoperation system with haptic feedback for the control of untethered soft grippers. The system is able to move and open/close the grippers by regulating the magnetic field and temperature in the workspace. Users can intuitively control the grippers using a grounded haptic interface, that is also capable of providing compelling force feedback information as the gripper interacts with the environment. The magnetic closed-loop control algorithm is designed starting from a Finite Element Model analysis. The electromagnetic model used is validated by a measurement of the magnetic field with a resolution of 0.1 mT and sampling rate of 6.8×10^6 samples/m^2. The system shows an accuracy in positioning the gripper of 0.08 mm at a velocity of 0.81 mm/s. The robustness of the control and tracking algorithms are tested by spraying the workspace with water drops that cause glares and related disturbances of up to 0.41 mm.**

I. Introduction

The majority of wireless small-scale robots presented in the literature have very limited manipulation capabilities, and none of the steering systems currently available enable a human operator to effectively and intuitively control the motion of dexterous sub-centimeter robots [1], [2]. To expand the possible applications of this type of robots and allow them to complete advanced functional tasks, researchers have recently focused on the design and development of miniaturized wireless motors with *grasping* capabilities. Being able to simultaneously grasp, move, and release micro-scale objects expands the applicability of such robots to several tasks and scenarios, including targeted biopsy, assembly, and minimally invasive surgery [3]–[5].

F. Ongaro and S. Misra are affiliated with the Surgical Robotics Laboratory, Dept. of Biomechanical Engineering, MIRA-Institute for Biomedical Technology and Technical Medicine, University of Twente, The Netherlands. S. Misra is also affiliated with the Dept. of Biomedical Engineering, University of Groningen and University Medical Centre Groningen, The Netherlands.

C. Pacchierotti and D. Prattichizzo are affiliated with the Dept. of Advanced Robotics, Istituto Italiano di Tecnologia, Genova, Italy. D. Prattichizzo is also affiliated with the Dept. of Information Engineering and Mathematics, University of Siena, Siena, Italy.

C. Yoon and D.H. Gracias are affiliated with the Dept. of Materials Science and Engineering, Johns Hopkins University, Baltimore, USA. D.H. Gracias is also affiliated with the Dept. of Chemical and Biomolecular Engineering, Johns Hopkins University, Baltimore, USA.

This research has received funding from the European Research Council (ERC) under the European Union's Horizon 2020 Research and Innovation programme (Grant Agreement #638428 - project *ROBOTAR*: Robot-Assisted Flexible Needle Steering for Targeted Delivery of Magnetic Agents), and from the European Union's Seventh Framework Programme FP7/2007-2013 (Grant Agreement #°601165 - project *WEARHAP* - WEARable HAPtics for humans and robots).

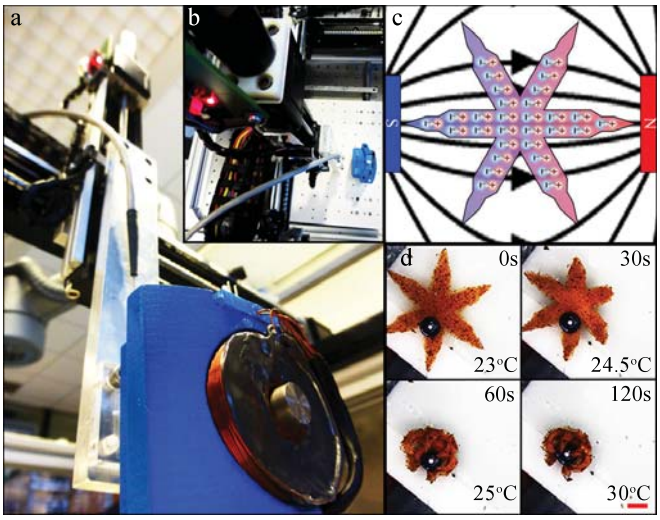

Fig. 1. *(a)* and *(b)* Images of the XYZ Cartesian robot used for field measurement. During the field measurements, the electromagnetic coils are supplied a current of 1 A. *(c)* A schematic representation of the induced magnetization of the grippers when exposed to electromagnetic fields. *(d)* Video snapshots of the soft grippers while closing. Scale-bar 0.8 mm.

However, the fabrication of small-scale actuators and power sources is still challenging. Therefore, stimuli responsive materials are expected to play an important role in the miniaturization of robotic grippers, since they naturally provide self-assembling and self-folding capabilities, with no need for specific end-effectors and bulky batteries. Self-folding stimuli-responsive soft robots can regulate their grasping configuration by converting environmental signals into mechanical ones. Because of this, they have been successfully utilized in a vast range of applications, such as drug delivery, diagnostics, and tissue engineering [6], [7].

Among stimuli-responsive soft materials, hydrogels, a class of porous soft-materials composed of a network of polymer chains, seem very promising. Hydrogels can be biocompatible and/or biodegradable, and can operate in aqueous environments. Further, recent advances in soft-lithography, photopatterning, and 3D printing allow hydrogel structures to be fabricated with micro-scale resolution. The use of soft bilayer devices for the encapsulation of several objects, such as cells [8], [9] or ferromagnetic particles [10], have drawn a lot of interest. In particular, untethered hydrogel grippers doped with biocompatible iron oxide offer the possibility to control both their motion and configuration [11], [12]. The temperature-induced differential stress in the bilayer structure enables the regulation of the grasping configuration of the gripper through temperature control,

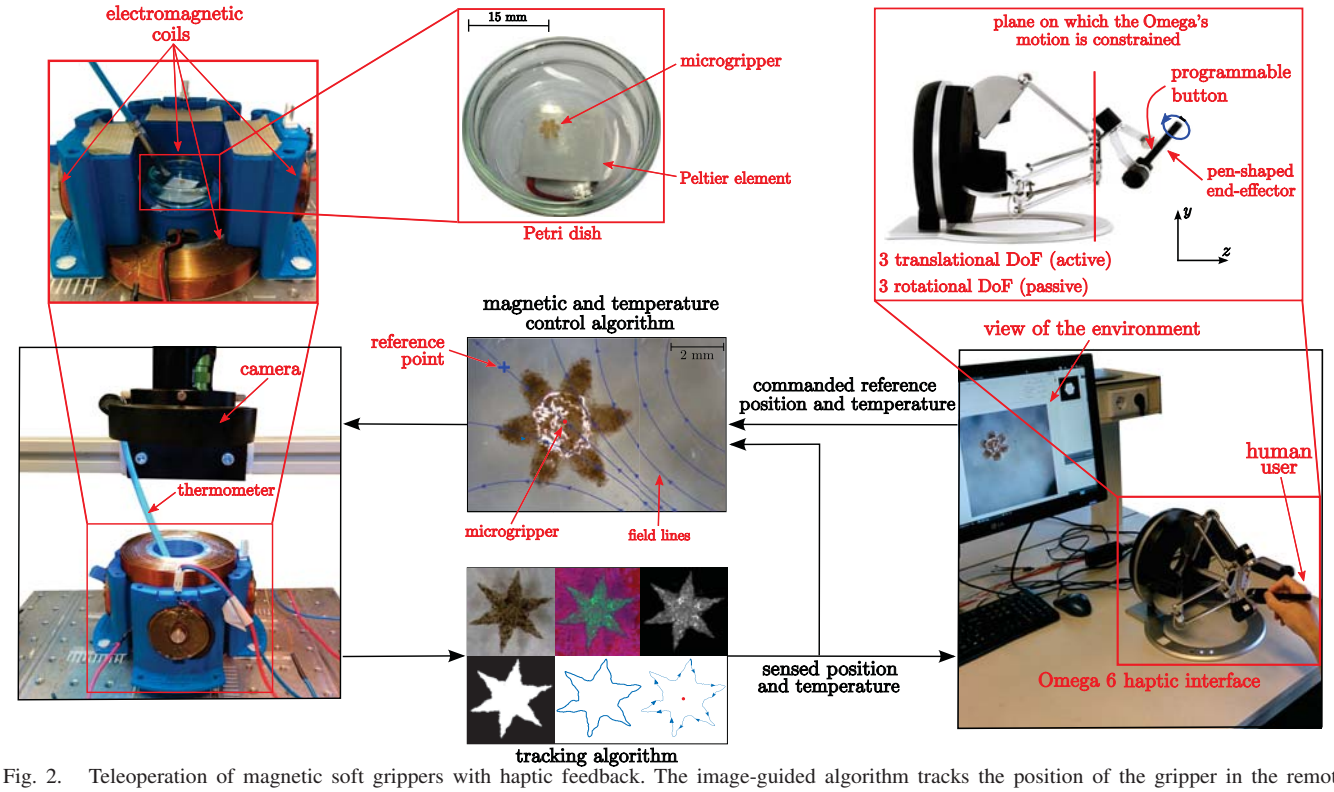

Fig. 2. Teleoperation of magnetic soft grippers with haptic feedback. The image-guided algorithm tracks the position of the gripper in the remote environment using a high-resolution camera and a Fourier-descriptors-based algorithm. A 6-DoF grounded haptic interface then provides the human operator with haptic feedback about the interaction of the gripper with the remote environment. At the same time, it enables the operator to intuitively control the reference position and grasping configuration of the gripper. Finally, magnetic and thermal control algorithms regulate the position and grasping configuration of the gripper.

while the ferromagnetic patterning allows wireless control of the position of the grippers through weak magnetic fields. The compliant mechanical properties of these substances could enable a delicate, flexible, and safe grasp of tissue, making the grippers suitable for medical procedures [11].

Researchers have proposed a variety of motion control approaches for ferromagnetic agents using iron-core electromagnetic coils and feedback extracted either from a microscopic vision system [1], [13], or from B-mode ultrasound images [14]. Further, a deep knowledge of such systems and of their rejection to environmental disturbances is a fundamental requirement to reach the robustness and precision that medical procedures would require. Finite Element Model (FEM) analysis is generally used for this purpose, since it allows the modeling of electromagnetic phenomena. However, these models can at most be as reliable as their experimental validation. Traditionally a small, low-density grid of points has been used for this purpose. This technique is sufficient for validating the magnetic field, but it is not sufficient for guaranteeing a reliable computation of the magnetic field gradient, on which the exerted magnetic force depends. The use of a large, high-density and high-resolution point-set for model validation would increase the knowledge of the system and its safety.

Moreover, for reasons of responsibility and public acceptance, it would be beneficial to provide a *human operator* with intuitive means for directly controlling the motion of grippers, especially when dealing with medical procedures [15], [16]. In these applications, the operator needs to receive sufficient information from the environment within which the controlled gripper is operating. This is possible through different types of information, that flow from the remote scenario to the human operator. They are usually a combination of visual and haptic stimuli. Visual feedback is already employed in several commercial telerobotic systems [17], and haptic feedback is widely believed to be a valuable tool in teleoperation [17]–[20] and manipulation [21]–[23]. In medical scenarios, haptic feedback has been demonstrated to improve performance in fine microneedle positioning [24], telerobotic catheter insertion [25], suturing simulation [26], cardiothoracic procedures [27], palpation [28], and cell injection systems [29]. The benefits of haptic feedback have been also shown in small-scale manipulation [21]–[23], [30], [31].

In this study, we present a magnetic teleoperation system with haptic feedback for the control of self-folding magnetic soft grippers. It enables human operators to wirelessly control a gripper during micromanipulation tasks, while providing them with haptic feedback on the interaction between the gripper and the remote environment. The electromagnetic model of our setup, is developed using FEM analysis and validated using a novel technique that makes use of an XYZ Cartesian robot to obtain a large, high-density and high-resolution set of measurements.

The paper is organized as follows: Section II describes the fabrication process, the electromagnetic and haptic systems, and their modeling and control. Section III presents and discusses the experimental evaluation of the system. Finally, Section IV concludes and provides directions for future work.

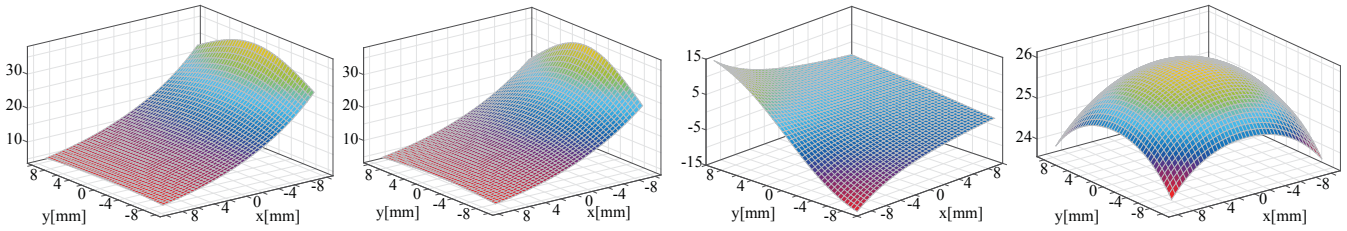

(a) $\|\mathbf{B}\|$ (mT) (b) B_x (mT) (c) B_y (mT) (d) B_z (mT)

Fig. 3. (a), (b) and (c) depict the FEM analysis of the field norm($\|\mathbf{B}\|$) and its x (B_x) and y (B_y) components of an iron-core coil placed at position (-23 mm; 0 mm) with respect to the graph. The coil is controlled with a current of 1 A. (d) shows the z (B_z) component of the field when controlling the air-core upper coil with a current of 1 A. Given the symmetry of the setup (Fig. 2), the field generated by the other coils can be obtained by properly rotating the ones shown here.

II. Experimental Setup

A. Fabrication of the Grippers

In order to fabricate the bilayer grippers, a 90% hydrolyzed polyvinyl alcohol (PVA) sacrificial layer is spin coated onto a Silicon (Si) wafer and then baked. Afterwards, an SU-8 film is spin coated above the PVA. When SU-8 is applied to the wafer through spin coating, the wafer is baked, photopatterned by exposure to ultraviolet (UV) light, then postbaked. After post baking the SU-8 layer, a pNIPAM layer is applied. The applied pNIPAM is exposed to UV light and unexposed regions are dissolved by rinsing with isopropyl alcohol. Then the wafer is submerged in DI water to obtain the grippers. These grippers have a star shape with dimension of 4 mm tip-to-tip, when fully opened, and the shape of a sphere with 0.4 mm radius, when closed (Fig. 1). The thickness of the SU-8 and pNIPAM-AAc layers are 21 μm and 34 μm, respectively.

B. Tracking system

In order to track the position of the hydrated grippers in the remote environment, we place an optical camera above the Petri dish hosting the environment (Fig. 2). The camera is a Blackfly 1.4 MP Color GigE PoE camera (Point Grey Research Inc., Canada), mounted on a Mitutoyo FS70 microscope unit (Mitutoyo, Kawasaki, Japan) using a Mitutoyo M Plan Apo 2 / 0.055 objective. This optical setup has an adjustable zoom with a maximum of 24X, a frame rate of 125 fps, and it is mounted on a mechanical track to enable precise focusing. A CCD sensor is used for recording, with a pixel width and height of 5.50 μm, providing a resolution of up to 0.50 μm.

We binarize the saturation channel of each extracted frame using a median filtering technique and applying an adaptive threshold. This binary image is then used to find the contours of the image. The Fourier descriptors of the contour are employed to detect the centroid of the gripper and measure the extent of its closure (Fig. 2). Finally, a standard Kalman filter is used to deal with uncertainties in the tracking [32].

C. Haptic system

The haptic feedback system uses a 6-DoF Omega haptic interface (Force Dimension, Switzerland) (Fig. 2). It is composed of a delta-based parallel kinematics structure that provides good closed-loop stiffness and high accuracy. The rotating wrist joint allows the user to also change the orientation of the pen-shaped end-effector. Translational degrees of freedom are active, while rotational degrees of freedom are passive. This haptic interface is also equipped with active gravity compensation to improve the teleoperation transparency and reduce the operator's fatigue. In this work we use the Omega 6 interface as an impedance haptic device. We measure the position of the end-effector, controlled by the human operator, to set the reference target position of the gripper. Through the same end-effector, we also provide the operator with force feedback from the remote environment. The scaling factor between master and slave systems is 0.2 in all directions, i.e., moving the end-effector of the Omega interface of 10 cm moves the gripper's reference position of 2 cm. The force to be provided is evaluated as detailed in Sec. III. The haptic control loop runs at 2 kHz. The Omega's pen-shaped end-effector is also equipped with a programmable button, which is used to activate/deactivate the temperature control on the Petri dish (Sec. II-D). When the temperature control is active, the human operator can set the target temperature of the environment by rotating the pen-shaped end-effector (Fig. 2-top right inset). As mentioned in Sec. I, controlling the temperature of the remote environment enable the operator to close and open the grippers.

D. Modeling and Control

Given the current position of the gripper, as estimated by the tracking algorithm, and the commanded reference position, as controlled by the grounded haptic interface, the control system moves the gripper using an array of six orthogonally-oriented iron-core electromagnets, with the objective of steering it toward the reference point. A Peltier element regulates the temperature of the water where the controlled gripper is floating, enabling the control of its grasping configuration (Fig. 2).

1) Position control using magnetic fields: As previously demonstrated in [13], [33], it is possible to map the currents $\mathbf{I} \in \mathbb{R}^{n\times 1}$ provided to n electromagnets into forces exerted on the considered gripper as

$$\mathbf{F}(\mathbf{p_m}) = (\mathbf{m}\cdot\nabla)\mathbf{B}(\mathbf{p_m}) = \mathbf{\Lambda}(\mathbf{m},\mathbf{p_m})\mathbf{I}\,, \qquad (1)$$

where $\mathbf{F}(\mathbf{p_m}) \in \mathbb{R}^{3\times 1}$ is the electromagnetic force exerted on the magnetic dipole with moment $\mathbf{m} \in \mathbb{R}^{3\times 1}$ at position $\mathbf{p_m} \in \mathbb{R}^{3\times 1}$, $\mathbf{B}(\mathbf{p_m}) \in \mathbb{R}^{3\times 1}$ is the magnetic flux density, ∇ is the gradient operation, and $\mathbf{\Lambda}(\mathbf{m},\mathbf{p_m}) \in \mathbb{R}^{3\times n}$ is the actuation matrix that maps the input currents into electromagnetic forces.

The force-current map $\mathbf{\Lambda}$ depends on $\mathbf{B}(\mathbf{p_m})$ and $\nabla\mathbf{B}(\mathbf{p_m})$. When the iron-cores are not saturated, we can express the field as

$$\mathbf{B}(\mathbf{p_m}) = \sum_{i=1}^{n} \widetilde{\mathbf{B}}_i(\mathbf{p_m}) I_i = \widetilde{\mathbf{B}}(\mathbf{p_m})\mathbf{I}, \tag{2}$$

where $\widetilde{\mathbf{B}}_i(\mathbf{p_m}) \in \mathbb{R}^{3\times1}$ is the current-to-field map, I_i is the current at the i^{th}-electromagnet, and $\widetilde{\mathbf{B}}(\mathbf{p_m}) \in \mathbb{R}^{3\times n}$ is the map between the magnetic flux density and the current vector $\mathbf{I}$. We used FEM analysis in order to map how the current vector $\mathbf{I}$ and $\mathbf{B}(\mathbf{p_m})$ are related (Fig. 3).

2) Magnetic fields validation: The values obtained from the FEM analysis have been successively compared with measurements of a 3-axis 3MH3 Teslameter (SENIS AG, Baar, Switzerland). This teslameter is able to measure the field components with a resolution of 0.1 mT. In the validation procedure the Hall probe is swept through the entire workspace by an XYZ Cartesian robot at constant velocity of 0.5 mm/sec [34], [35]. The validation is performed on 1523 samples in the 1.2×1.2 cm workspace for a resulting sampling rate of 6.8×10^6 samples/m^2. The root mean square and standard deviation of the magnitude and orientation mismatches between FEM analysis and measurements are $7.4\times10^{-3}\pm2.2$ mT and $4.2\pm2.6°$, respectively. Compared to the traditional measurement of few tens of points in a grid, the high-density nature of the samples of this novel technique offer more reliable results, especially when these have to be derived to obtain the field gradient. The validated $\widetilde{\mathbf{B}}(\mathbf{p})$ is fitted to a quadratic Lowess function using MATLAB (MathWorks Inc., Natick, United States) (Tab. I).

In order to evaluate $\mathbf{m}$, we assume the grippers to have a uniform iron oxide distribution. This allows us to consider $\mathbf{m}$ as the superposition of three pairs of counterposed two-tip dipoles, $\mathbf{m}_{tips} \in \mathbb{R}^{3\times1}$ (Fig. 1). We remove 4 out of 6 counterposed tips from a gripper and use the *U-turn* technique to experimentally measure $||\mathbf{m}_{tips}||$ [36]. This results to be 3.5×10^{-8} Am^2, with the same direction as the vector separating the two poles, $\mathbf{d} \in \mathbb{R}^{3\times1}$, as can be inferred from $\mathbf{m}_{tips} = p\mathbf{d} = |\mathbf{m}_{tips}|\frac{\mathbf{d}}{|\mathbf{d}|}$, where $p \in \mathbb{R}$ is the magnetic pole strength [37]. The magnetic dipole moment of the gripper is computed by summing up the three rotated two-tip dipoles. Consequently, the resulting $\mathbf{m}$ has a magnitude of 7×10^{-8} Am^2 and a direction that depends on the gripper's orientation. Note that the adopted technique overestimates the magnetic dipole moment of the central overlapping part. However, this overestimation is assumed to have a negligible effect due to the small magnitude of $\mathbf{d}$.

TABLE I

QUALITY INDICES FOR EACH COMPONENT OF THE MAGNETIC FIELD FOR THE OBTAINED FITTING FUNCTION. THE TABLE REPORTS SUM SQUARED ERROR (SSE), R-SQUARE, ADJUSTED R-SQUARE, AND ROOT MEAN SQUARE ERROR (RMSE).

	SSE	R-square	Adj. R-square	RMSE
$\mathbf{B}_x$	4.7×10^{-7} T	1.0000	1.000	6.7×10^{-6} T
$\mathbf{B}_y$	2.9×10^{-7} T	1.0000	1.000	5.3×10^{-6} T
$\mathbf{B}_z$	8.2×10^{-7} T	0.9998	0.999	7.8×10^{-6} T

We used this estimation of the magnetic dipole moment of the grippers and the validated model of the setup for the design of a closed-loop motion controller. The regulation of the input currents is implemented using a Multi-Input Multi-Output (MIMO) Proportional Integral Derivative (PID) control [33]. The control uses $\mathbf{\Lambda}^+$, i.e., the Moore-Penrose pseudo-inverse of $\mathbf{\Lambda}$, to map the forces into currents for our six electromagnets. In order to couple the dynamics on different axes, the control actions are set to respect conditions

$$F_x \leqslant \frac{e_x}{|\mathbf{e}|}F_M, \quad F_y \leqslant \frac{e_y}{|\mathbf{e}|}F_M, \tag{3}$$

where F_x and F_y are the forces exerted on the x and y axes respectively, F_M is the estimated maximum exertable force, and $\mathbf{e} = [e_x \;\; e_y]$ is the position error.

3) Grasping configuration control using a Peltier element: The self-folding capabilities of the soft grippers can be controlled using thermal stimuli [11]. For this purpose, we regulate the temperature of the water wherein the grippers are floating using a Peltier element, which is able to produce both positive and negative temperature differentials between its two faces. The element is directly attached to the bottom of the Petri dish, as shown in the left hand side of Fig. 2. Moreover, in order to compensate for Joule effects, an aluminum heat-sink is attached to the outer face of the element. A closed-loop temperature control is implemented using an Arduino Uno board (Arduino, Ivrea, Italy) and a thermometric probe. The regulator reads the water temperature from the probe and receives the target temperature from the haptic interface (Sec. II-C). These inputs are then fed to a proportional controller that determines the current for the Peltier element. The system is able to reach the reference temperature at approximately 10°C per minute.

III. EXPERIMENTAL EVALUATION

In order to evaluate the effectiveness of our magnetic teleoperation system, we carried out three experiments. The first experiment evaluates the nominal performance of our magnetic control system in positioning a soft gripper, in terms of precision and speed. The second experiment introduces impulse-like disturbances to the system in order to analyze the robustness of the tracking and control algorithms. Finally, the third experiment verifies the effectiveness of the integrated haptic-enabled teleoperation system in a complex pick-and-place task. *Please refer to the attached video for these experiments.*

The nominal performance of the closed-loop magnetic position controller is assessed in 120 motion control experimental trials, which consist of point-to-point positioning tasks (40 trials) and tracking of circular and square trajectories (80 trials). The circular trajectories have a radius of 3 mm, while the square trajectories have a side of 6 mm. Eight different grippers are used. The grippers move with an average velocity of 0.81 ± 0.12 mm/s and with a positioning error of 0.08 ± 0.05 mm (Fig. 4).

Successively, the robustness of the control and tracking algorithms is evaluated. For this purpose, the above presented

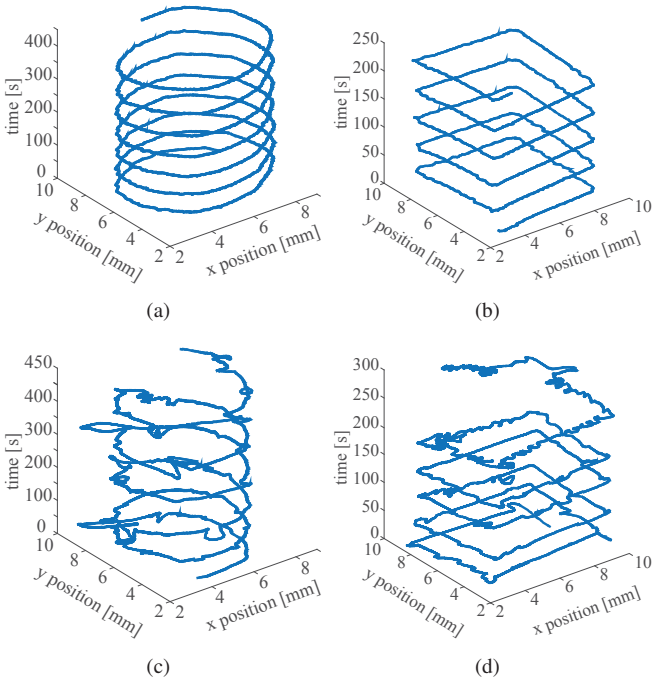

Fig. 4. Representative closed-loop motion control experimental results. Both trajectories are centered in (6 mm; 6 mm) with respect to the coordinates in the graph. In *a)* and *b)* the system operates in nominal conditions. In *c)* and *d)* an impulse-like disturbance is introduced every 3 s.

trajectory-following experiments are repeated while, every three seconds, water drops of 75 μl strike the water surface from heights between 3 mm and 10 mm. The drops generate ripples that cause displacements of the gripper of up to 0.41 mm. The wavelets also reflect the light from the camera disturbing the tracking procedure. Circular and square trajectories are followed in 30 trials with 3 different grippers. In these experiments, the average velocity remains consistent with the previous trials (0.84±0.22 mm/s). However, the average error increases to 0.25±0.24 mm (Fig. 4). Even if the disturbance causes numerous glares and high jerks of the gripper, the tracker is always able to robustly trace the grippers.

Also the teleoperation capabilities of the grippers are evaluated. For this purpose, the grippers are used to pick up a 0.5 mm-sized spherical polystyrene object (Polysciences, Warrington, USA) from the ground and release it on a targeted location, using the integrated haptic-enabled teleoperation system shown in Fig. 2. A 0.5 mm thick acrylic wall is present in the workspace and has to be avoided during this procedure. The pick up and drop-off locations are chosen randomly. Five subjects (3 males, 2 female, age range 21 - 28 years) take part in the experiment. The Omega haptic interface provides the subject with haptic feedback about the collisions of the reference point with the obstacle and about the inertia of the gripper. The haptic force responsible for rendering collisions of the reference point with the obstacle, is evaluated according to the popular god-object model, and the obstacle is modeled as a spring-damper system ($k = 1000$ N/m, $b = 5$ Ns/m) [38]. Moreover, the Omega also provides an attractive haptic force that keeps the reference point close to the controlled gripper, modeled as if a spring-damper system is placed between the reference point, controlled by the Omega, and the gripper ($k = 200$ N/m, $b = 5$ Ns/m). The subject thus feels an opposite force when trying to penetrate the obstacle and when moving the reference point away from the gripper. The position of the gripper is regulated by the magnetic position control, as described in Sec. II-D.1, and its grasping configuration is regulated by the temperature control, as described in Sec. II-D.3. The Omega interface enables the human operator to set both the reference position and grasping configuration of the gripper, as described in Sec. II-C. Subjects are required to complete the pick-and-place task 6 times, either with or without haptic feedback.

Results show a completion time of 25.2 ± 2.80 s, an average path length of 22.4 ± 4.00 mm, a drop-off error of 0.88 ± 0.32 mm for the condition providing haptic feedback, with an improvement of 21%, 22%, and 13% with respect to the condition providing no haptic feedback, respectively. Finally, subjects are also asked to rate the perceived effectiveness of both conditions in a scale from 0 to 10, and to choose the condition they mostly prefer. The condition providing haptic feedback is preferred by all subjects, who rated it 6.3 out of 10. The condition providing no force feedback is rated 3.7 out of 10.

IV. Conclusions

This work presents a novel magnetic teleoperation system with haptic feedback for the wireless control of soft magnetic grippers. An image-guided algorithm tracks the position of the gripper in the remote environment. A 6-DoF grounded haptic interface provides the human operator with haptic feedback about the interaction of the gripper with the remote environment, and enables the operator to control the reference position and grasping configuration of the gripper. FEM analysis is used to devise a model that maps the currents at the electromagnets to the forces applied to the controlled gripper. The validity of the our model is experimentally demonstrated using a large, high-density and high-resolution set of measurements obtained by sweeping a 3-axis Teslameter in the workspace, by means of an XYZ Cartesian robot.

The resulting model is used to develop a closed-loop motion control algorithm. The performance of this control in nominal conditions is assessed in 120 trials. The system shows an accuracy in positioning the gripper of 0.08 mm at a velocity of 0.81 mm/s. In order to evaluate the robustness of the control and tracking algorithm, thirty additional trials are performed in the presence of visual and position impulse-like disturbances. In this scenario, the system is able to maintain an average error of 0.25 mm when affected by periodic disturbances of up to 0.41 mm. We also perform pick-and-place experiments where five users are asked to pick a micro-scale object from the bottom of the dish, transport it, and release it at a predetermined location using the integrated haptic-enabled teleoperation system. Results show an accuracy in positioning the micro-scale object of 0.88 mm. All subjects are able to successfully complete the given task.

In the near future, we will investigate the practical translational aspects of the proposed teleoperation system for

biomedical applications. This include the use of smaller scale grippers, the study of against-the-flow motion, and the use of clinically-compatible imaging, such as ultrasound, which is consistent with the ultrasound-visibility of the fabrication materials [14]. Moreover, we will test different types of haptic stimuli (e.g., vibratory, skin-stretch, pin-arrays) and sensory substitution techniques (e.g., visual, audio), with the objective of improving the results registered in this work. Future applications of the system include targeted drug delivery of micro-sized agents and nanocapsules, as well as minimally-invasive surgery and small-scale manipulation of artificial objects.

REFERENCES

[1] I. S. M. Khalil, V. Magdanz, S. Sanchez, O. G. Schmidt, and M. S, "Three-dimensional closed-loop control of self-propelled microjets," *Appl. Phys. Lett.*, vol. 103, no. 17, p. 172404, 2013.

[2] W. Gao, R. Dong, S. Thamphiwatana, J. Li, W. Gao, L. Zhang, and J. Wang, "Artificial micromotors in the mouses stomach: A step toward in vivo use of synthetic motors," *ACS Nano*, vol. 9, no. 1, pp. 117–123, 2015.

[3] S. Tottori, L. Zhang, F. Qiu, K. K. Krawczyk, A. Franco-Obregón, and B. J. Nelson, "Magnetic helical micromachines: fabrication, controlled swimming, and cargo transport," *Adv. Mater.*, vol. 24, no. 6, pp. 811–816, 2012.

[4] E. Diller and M. Sitti, "Three-dimensional programmable assembly by untethered magnetic robotic micro-grippers," *Adv. Funct. Mater.*, vol. 24, no. 28, pp. 4397–4404, 2014.

[5] J. C. Kuo, H. W. Huang, S. W. Tung, and Y. J. Yang, "A hydrogel-based intravascular microgripper manipulated using magnetic fields," *Sensors and Actuators A: Physical*, vol. 211, pp. 121–130, 2014.

[6] J. S. Randhawa, K. E. Laflin, N. Seelam, and D. H. Gracias, "Microchemomechanical systems," *Advanced Functional Materials*, vol. 21, no. 13, pp. 2395–2410, 2011.

[7] E. Gultepe, J. S. Randhawa, S. Kadam, S. Yamanaka, F. M. Selaru, E. J. Shin, A. N. Kalloo, and D. H. Gracias, "Biopsy with thermally-responsive untethered microtools," *Adv. Mater.*, vol. 25, no. 4, pp. 514–519, 2013.

[8] K. Malachowski, J. Breger, H. R. Kwag, M. O. Wang, J. P. Fisher, F. M. Selaru, and D. H. Gracias, "Stimuli-responsive theragrippers for chemomechanical controlled release," *Angewandte Chemie*, vol. 126, no. 31, pp. 8183–8187, 2014.

[9] M. Jamal, S. S. Kadam, R. Xiao, F. Jivan, T.-M. Onn, R. Fernandes, T. D. Nguyen, and D. H. Gracias, "Bio-origami hydrogel scaffolds composed of photocrosslinked peg bilayers," *Advanced Healthcare Materials*, vol. 2, no. 8, pp. 1142–1150, 2013.

[10] S. Fusco, M. S. Sakar, S. Kennedy, C. Peters, R. Bottani, F. Starsich, A. Mao, G. A. Sotiriou, S. Pané, S. E. Pratsinis, *et al.*, "An integrated microrobotic platform for on-demand, targeted therapeutic interventions," *Adv. Mater.*, vol. 26, no. 6, pp. 952–957, 2014.

[11] J. C. Breger, C. Yoon, R. Xiao, H. R. Kwag, M. O. Wang, J. P. Fisher, T. D. Nguyen, and D. H. Gracias, "Self-folding thermo-magnetically responsive soft microgrippers," *ACS App. Mater. & Interfaces*, vol. 7, no. 5, pp. 3398–3405, 2015.

[12] S. Miyashita, S. Guitron, M. Ludersdorfer, C. R. Sung, and D. Rus, "Untethered miniature origami robot that self-folds, walks, swims, and degrades," in *Proc. of the IEEE Int. Conf. on Robotics and Automation (ICRA)*, pp. 1490–1496, May 2015.

[13] M. P. Kummer, J. J. Abbott, B. E. Kratochvil, R. Borer, A. Sengul, and B. J. Nelson, "Octomag: An electromagnetic system for 5-dof wireless micromanipulation," *IEEE Trans. on Robotics*, vol. 26, no. 6, pp. 1006–1017, 2010.

[14] A. Sanchez, V. Magdanz, O. G. Schmidt, and S. Misra, "Magnetic control of self-propelled microjets under ultrasound image guidance," in *Proc. 5th IEEE RAS & EMBS Int. Conf. on Biomedical Robotics and Biomechatronics*, pp. 169–174, 2014.

[15] J. Troccaz and Y. Delnondedieu, "Semi-active guiding systems in surgery. a two-dof prototype of the passive arm with dynamic constraints (PADyC)," *Mechatronics*, vol. 6, no. 4, pp. 399–421, 1996.

[16] C. Pacchierotti, M. Abayazid, S. Misra, and D. Prattichizzo, "Teleoperation of steerable flexible needles by combining kinesthetic and vibratory feedback," *IEEE Trans. on Haptics*, vol. 7, no. 4, pp. 551–556, 2014.

[17] C. Pacchierotti, *Cutaneous haptic feedback in robotic teleoperation*. Springer Series on Touch and Haptic Systems, 2015.

[18] A. M. Okamura, "Methods for haptic feedback in teleoperated robot-assisted surgery," *Industrial Robot: An Int. Journal*, vol. 31, no. 6, pp. 499–508, 2004.

[19] C. Pacchierotti, L. Meli, F. Chinello, M. Malvezzi, and D. Prattichizzo, "Cutaneous haptic feedback to ensure the stability of robotic teleoperation systems," *The Int.l Journal of Robotics Research*, vol. 34, no. 14, pp. 1773–1787, 2015.

[20] A. M. Jarc and I. Nisky, "Robot-assisted surgery: an emerging platform for human neuroscience research," *Frontiers in Human Neuroscience*, vol. 9, p. 315, 2015.

[21] N. Ando, P. Korondi, and H. Hashimoto, "Development of micromanipulator and haptic interface for networked micromanipulation," *IEEE/ASME Trans. on Mechatronics*, vol. 6, no. 4, pp. 417–427, 2001.

[22] A. Bolopion and S. Régnier, "A review of haptic feedback teleoperation systems for micromanipulation and microassembly," *IEEE Trans. on Automation Science and Engineering*, vol. 10, no. 3, pp. 496–502, 2013.

[23] C. Pacchierotti, V. Magdanz, M. Medina-Sánchez, O. G. Schmidt, D. Prattichizzo, and S. Misra, "Intuitive control of self-propelled microjets with haptic feedback," *Journal of Micro-Bio Robotics*, vol. 10, no. 1-4, pp. 37–53, 2015.

[24] S. Salcudean, S. Ku, and G. Bell, "Performance measurement in scaled teleoperation for microsurgery," in *Proc. of the First Joint Conf. on Computer Vision, Virtual Reality and Robotics in Medicine and Medial Robotics and Computer-Assisted Surgery*, pp. 789–798, 1997.

[25] A. Kazi, "Operator performance in surgical telemanipulation," *Presence: Teleoperators & Virtual Environments*, vol. 10, no. 5, pp. 495–510, 2001.

[26] L. Moody, C. Baber, and T. N. Arvanitis, "Objective surgical performance evaluation based on haptic feedback," *Studies in health technology and informatics*, vol. 85, pp. 304–310, 2002.

[27] C. W. Kennedy, T. Hu, J. P. Desai, A. S. Wechsler, and J. Y. Kresh, "A novel approach to robotic cardiac surgery using haptics and vision," *Cardiovascular Engineering*, vol. 2, no. 1, pp. 15–22, 2002.

[28] C. Pacchierotti, D. Prattichizzo, and K. J. Kuchenbecker, "Cutaneous feedback of fingertip deformation and vibration for palpation in robotic surgery," *IEEE Trans. on Biomedical Engineering*, vol. 63, pp. 278–287, 2015.

[29] A. Pillarisetti, M. Pekarev, A. Brooks, and J. Desai, "Evaluating the effect of force feedback in cell injection," *IEEE Trans. on Automation Science and Engineering*, vol. 4, no. 3, pp. 322–331, 2007.

[30] M. Mehrtash, N. Tsuda, and M. B. Khamesee, "Bilateral macro–micro teleoperation using magnetic levitation," *IEEE/ASME Trans. on Mechatronics*, vol. 16, no. 3, pp. 459–469, 2011.

[31] A. Ghanbari, B. Horan, S. Nahavandi, X. Chen, and W. Wang, "Haptic microrobotic cell injection system," *IEEE Systems Journal*, vol. 8, no. 2, pp. 371–383, 2014.

[32] P. R. Belanger, P. Dobrovolny, A. Helmy, and X. Zhang, "Estimation of angular velocity and acceleration from shaft-encoder measurements," *The Int. Journal of Robotics Research*, vol. 17, no. 11, pp. 1225–1233, 1998.

[33] I. S. M. Khalil, L. Abelmann, and S. Misra, "Magnetic-based motion control of paramagnetic microparticles with disturbance compensation," *IEEE Trans. on Magnetics*, vol. 50, no. 10, pp. 1–10, 2014.

[34] G. J. Vrooijink, M. Abayazid, and S. Misra, "Real-time three-dimensional flexible needle tracking using two-dimensional ultrasound," in *Proc. of IEEE Int. Conf. on Robotics and Automation (ICRA)*, pp. 1688–1693, 2013.

[35] G. J. Vrooijink, M. Abayazid, S. Patil, R. Alterovitz, and S. Misra, "Needle path planning and steering in a three-dimensional non-static environment using two-dimensional ultrasound images," *The Int. Journal of Robotics Research*, vol. 33, no. 10, pp. 1361–1374, 2014.

[36] A. S. Bahaj, P. A. B. James, and F. D. Moeschler, "An alternative method for the estimation of the magnetic moment of non-spherical magnetotactic bacteria," *IEEE Trans. on Magnetics*, vol. 32, no. 5, pp. 5133–5135, 1996.

[37] W. F. Brown, "Magnetostatic principles," in *Ferromagnetism*, North-Holland Amsterdam, 1962.

[38] C. B. Zilles and J. K. Salisbury, "A constraint-based god-object method for haptic display," in *Proc. of the IEEE Int. Conf. on Human Robot Interaction and Cooperative Robots*, vol. 3, pp. 146–151, 1995.